Application of Spectral Element Method for Solving Problems of Geomechanics and Soil Mechanics in CAE Fidesys

Anatoly Vershinin[1,a)], Michael Cartsev[2,b)], Viktor Kozlov[2,c)], Vladimir Levin[1,d)]

[1]*Lomonosov Moscow State University*
[2]*Fidesys LLC*

[a)] Corresponding author: versh1984@mail.ru
[b)] cartsev@cae-fidesys.com
[c)] v.kozlov@cae-fidesys.com
[d)] v.a.levin@mail.ru

Abstract. The research is devoted to an overview of mathematical models and applied problems in mathematical modeling of geomechanical processes occurring in rocks. These problems were simulated in CAE Fidesys, which allows solving static and dynamic problems of geomechanics and geotechnics using spectral element method (SEM) of variable order of space approximation. Examples of solved problems with Mohr-Coulomb and Hoek-Brown mathematical models used in practice to describe the deformation of rocks and soils are considered. Simulation of plastic shear bands and their dependence on material properties is analyzed. Obtained numerical results are verified by comparison with the analytical solutions.

INTRODUCTION

Plastic shear bands are narrow zones within a solid body that are subject to uncontrolled strain growth due to plastic strain localization. Identifying the onset of such bands and investigating their development mechanisms is an important task in continuum mechanics of deformable solid [1–4]. Cohesive crack models [5–7] represent first attempts to study plastic shear bands. At present, numerical methods—most notably the finite element method (FEM) [6–12]—are widely used to analyze such states.

It is well known that one of the challenges of numerical simulation of plastic shear bands formation and development is their sensitivity to mesh parameters [13]. The development of the finite element method and its modifications, namely the spectral element method (SEM) [14–15], makes it possible to achieve a higher accuracy and a numerical convergence of strains localization just by increasing the order of the spectral element without mesh refinement [25].

This paper presents an analysis of several geomechanical problems solved using SEM. The first example, in addition to comparing the numerical solution with an analytical one, aims to benchmark SEM against FEM. In subsequent problems, SEM is applied exclusively as a powerful numerical solution method.

MATHEMATICAL MODELS

Let **B** be a solid body occupying the domain Ω in three-dimensional Euclidean space $\mathbf{E}^3$ with a closed boundary $\partial\Omega$.

The equation of motion for a continuum body can be written as [16]:

$$\rho \frac{d^2\vec{u}}{dt^2} = \vec{\nabla} \cdot \underset{\sim}{\sigma} + \rho\vec{f} \quad \forall \vec{x} \in \Omega, \tag{1}$$

where $\underset{\sim}{\sigma}=\underset{\sim}{\sigma}(\vec{x})$– Cauchy stress tensor, $\vec{u}=\vec{u}(\vec{x})$– displacement vector, $\vec{f}$– vector of external body forces, ρ– density.

To describe deformations, the Cauchy–Green strain tensor is used [17]:

$$\underset{\sim}{\varepsilon}=\frac{1}{2}\left(\overrightarrow{\nabla}\vec{u}+\vec{u}\overrightarrow{\nabla}\right). \tag{2}$$

The relationship between the stress and strain tensors is governed by the generalized Hooke's law [18]:

$$\underset{\sim}{\sigma}=D_e:\underset{\sim}{\varepsilon}_e. \tag{3}$$

For isotropic materials, the fourth-order elasticity tensor can be expressed in general form:

$$D_e=2G\,I_S+A\left(K-\frac{2G}{3}\right)\underset{\sim}{I}\otimes\underset{\sim}{I}, \tag{4}$$

where G and K are the shear and bulk moduli, A is a coefficient depending on the chosen theory, I_S is the fourth-order identity tensor, and $\underset{\sim}{I}$ is the second-order identity tensor.

Assuming the thickness of the considered models along the basis vector $\vec{e}_3$ is constant and sufficiently large, the plane strain theory can be applied. Equation (3) is then supplemented with the following conditions:

$$\begin{gathered}\varepsilon_{i3}=\varepsilon_{3i}=0\\ \sigma_{i3}=\sigma_{3i}=0, i\neq 3.\\ A=1\end{gathered} \tag{5}$$

In plasticity theory, the domainΩ is divided into elastic and plastic regions. In the elastic region, the following condition holds [19]

$$F(\underset{\sim}{\sigma})<0, \tag{6}$$

where $F(\underset{\sim}{\sigma})$ is the yield criterion, chosen individually for each model. Equations (1-5) are sufficient to describe the elastic region. In the plastic region, condition (6) is violated, and the stress–strain state is additionally governed by the relation:

$$F(\underset{\sim}{\sigma})=0. \tag{7}$$

Under the assumption of small strain theory, the strain rate is additively decomposed into elastic and plastic parts [20]:

$$\dot{\underset{\sim}{\varepsilon}}=\dot{\underset{\sim}{\varepsilon}}_e+\dot{\underset{\sim}{\varepsilon}}_p. \tag{8}$$

The plastic strain rate is obtained from the flow rule:

$$\dot{\underset{\sim}{\varepsilon}}_p=\dot{\gamma}\frac{\partial Q}{\partial\underset{\sim}{\sigma}}, \tag{9}$$

where $Q(\underset{\sim}{\sigma})$ is the plastic potential which is generally different from $F(\underset{\sim}{\sigma})$, i.e. non-associative plasticity is considered [26-28].

Mohr–Coulomb Model

To correctly describe plastic deformations in rocks, a mathematical model must be sensitive to hydrostatic pressure [26-28]. A well-known example of such a model is the Mohr–Coulomb yield criterion [22], expressed as:

$$\tau=c-\sigma_n\tan\phi, \tag{10}$$

where $\phi$is internal friction angle, $c$is cohesion, $\sigma_n$is normal stress, $\tau$is shear stress.

In terms of principal stresses, this equation takes the form (Fig.1):

$$F=(\sin\phi+1)\sigma_1+(\sin\phi-1)\sigma_3-2c\cos\phi=0. \tag{11}$$

The plastic potential has a form similar to that of the yield surface, but instead of the internal friction angle ϕ the dilatancy angle ψ is used:

$$Q=(\sin\psi+1)\sigma_1+(\sin\psi-1)\sigma_3-2c\cos\psi=0. \tag{12}$$

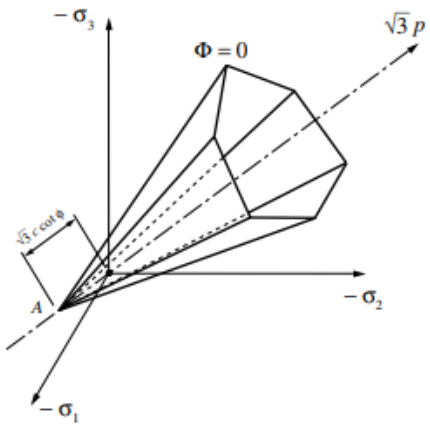

FIGURE 1. Mohr-Coulomb yield surface

Hoek–Brown Model

The Mohr-Coulomb model generally cannot fully describe the behavior of a rock due to the very wide range of stress levels occurring within it. It is also known that rocks often exhibit significant tensile strength. The Hoek-Brown yield criterion, widely used for modeling geomechanical processes [29], can be written in terms of the principal stresses (Fig. 2):

$$F=\sigma_1 - \sigma_3 - \sigma_{ci}\left(s - m_b \frac{\sigma_1}{\sigma_{ci}}\right)^a =0, \tag{13}$$

where the parameterss, m_b, a are defined as:

$$\begin{gathered} m_b=m_i e^{(\mathrm{GSI}-100)/(28-4D)} \\ s=e^{(\mathrm{GSI}-100)/(9-3D)} \\ a=0.5+\frac{e^{-\mathrm{GSI}/15}-e^{-20/3}}{6} \end{gathered}, \tag{14}$$

where σ_{ci} is an uniaxial compressive strength of the intact rock,GSI is Geological Strength Index, m_i is a material constant of intact rock, D is disturbance factor.

For the Hoek–Brown model, the plastic potential $Q(\underset{\sim}{\sigma})$ coincides exactly with the yield function $F(\underset{\sim}{\sigma})$.

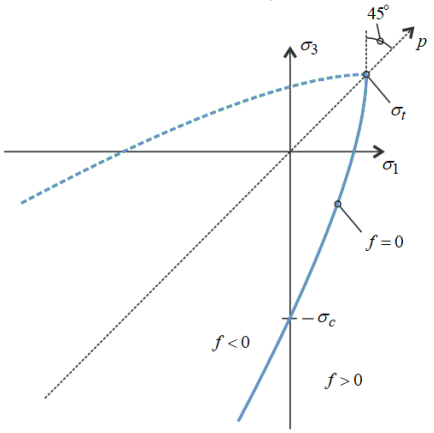

FIGURE 2. Projection of the Hoek-Brown yield surface on the $\sigma_1 - \sigma_3$ plane

CALCULATION RESULTS

End-loaded Tapered Cantilever

The failure of a tapered cantilever under shear loading is considered (Fig. 3).

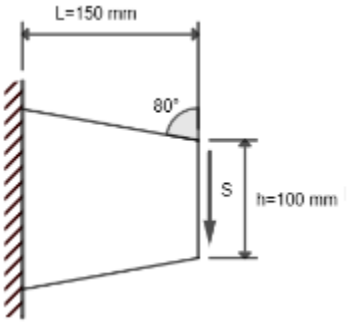

Young's modulus E = 210 GPa
Poisson's ratio ν = 0.3
Rock disturbance factor D = 0.3
Intact rock parameter $m_i = 1$
Geological Strength Index GSI = 70
Uniaxial compressive strength of intact rock $\sigma_{ci} = 2.4$ GPa

FIGURE 3. Computational model of the cantilever

Figure 4 presents the dependence between the vertical displacement of the loaded boundary of the cantilever and the applied load S. The graph indicates the maximum load at which the cantilever fails (uncontrolled displacement growth). Figure 5 shows the plastic strain field.

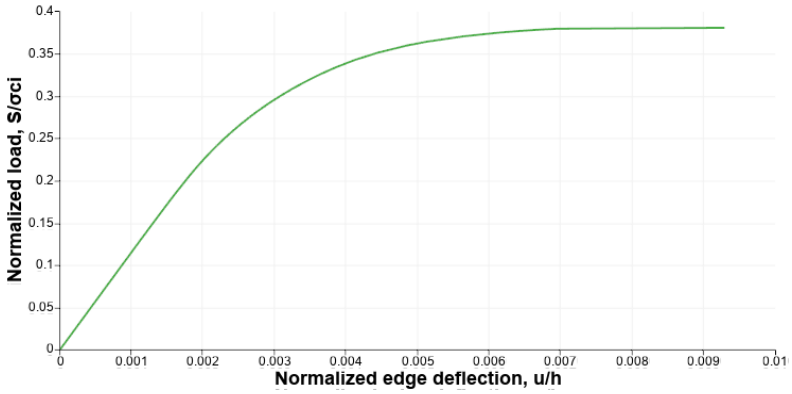

FIGURE 4. Load–displacement curve of the cantilever end

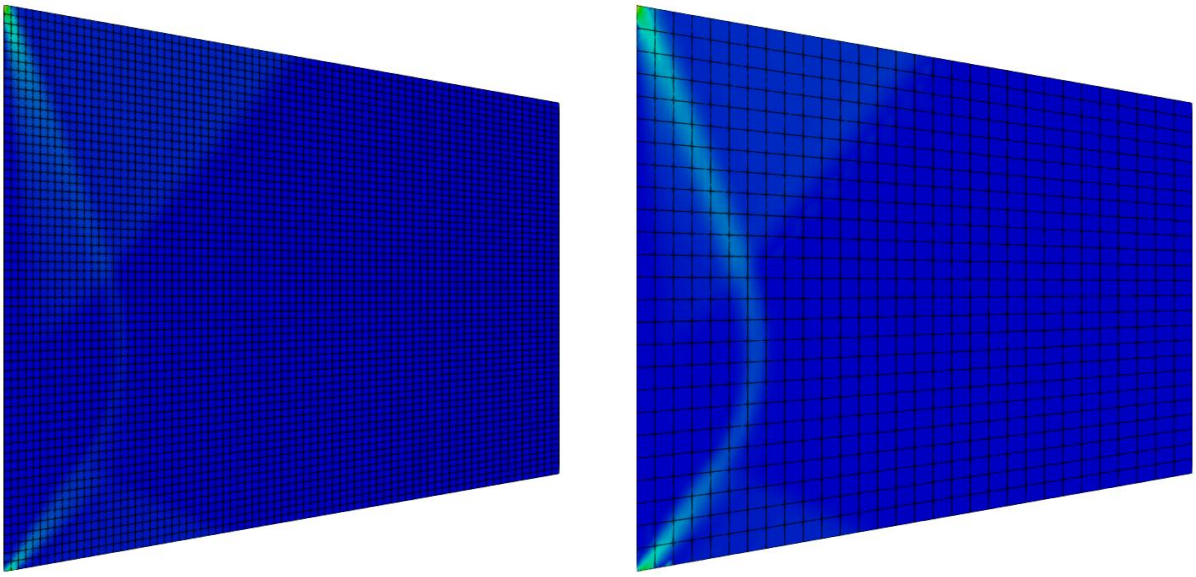

(a) (b)

FIGURE 5. Comparison of plastic strain fields for FEM (a) and SEM (b)

Clearly visible shear bands correspond to the analytical solution proposed by Green [21]. The spectral element method demonstrates a sharper localization pattern of the shear bands compared to the finite element method, while requiring fewer elements.

Strip-footing Collapse

Deformation of the soil media under the indentation of a rigid stamp is considered (Fig. 6).

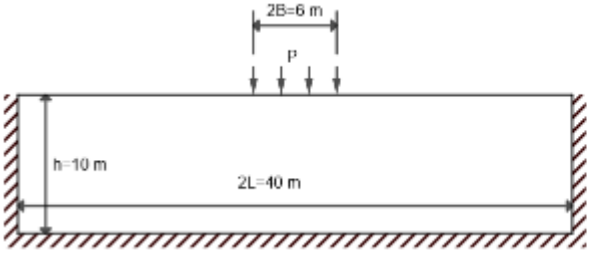

Young's modulus E = 257.143 MPa
Poisson's ratio ν = 0.285714
Rock disturbance factor D = 0
Intact rock parameter $m_i = 0$
Geological Strength Index GSI = 100
Uniaxial compressive strength of intact rock $\sigma_{ci} = 1$ MPa

FIGURE 6. Computational model of strip-footing

The graph in Fig. 7 shows excellent convergence to the theoretical value of the ultimate (critical) load:

$$\frac{P_{\text{lim}}}{\sigma_{\text{ci}}} \approx 2.57. \tag{15}$$

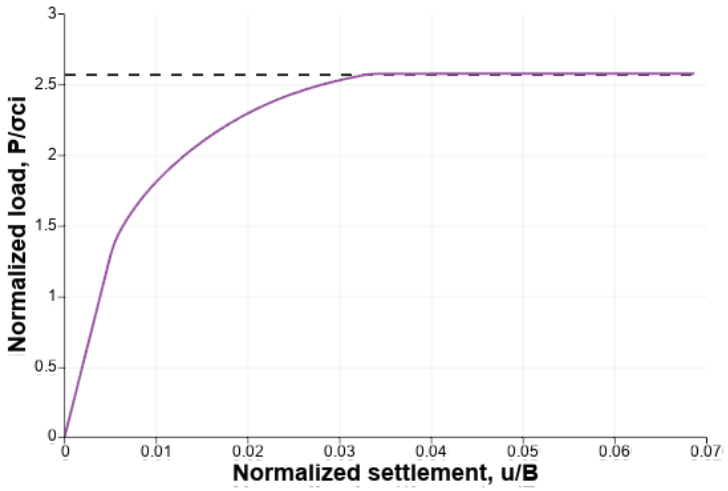

FIGURE 7. A pressure–displacement curve for the stamp indentation into the soil media

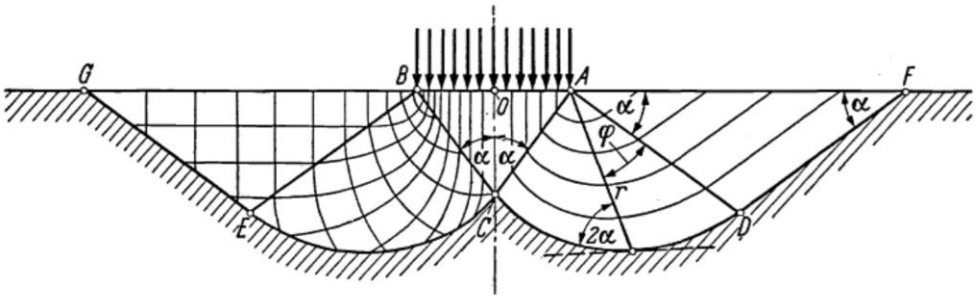

(a)

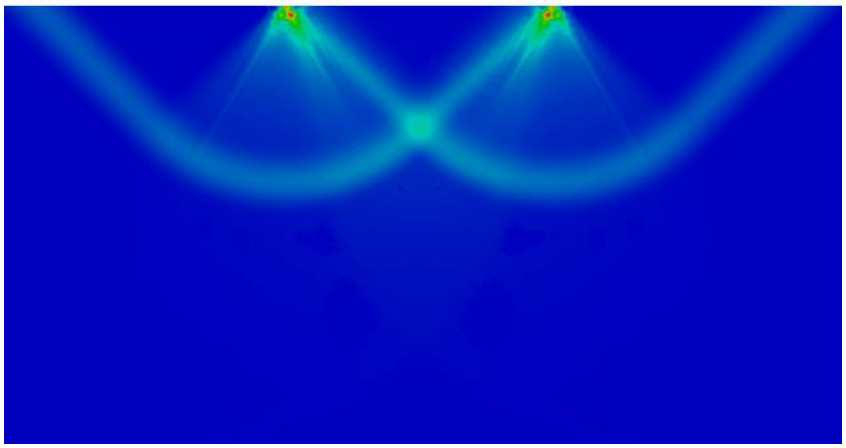

(b)

FIGURE 8. Plastic shear bands analytical (a) and numerical by SEM (b) due to stamp indentation

The shear bands at Fig. 8 demonstrate close agreement with the analytical solution presented by Prandtl and Hill [22].

Slope Stability

The deformation of a slope under its own weight is considered (Fig. 9).

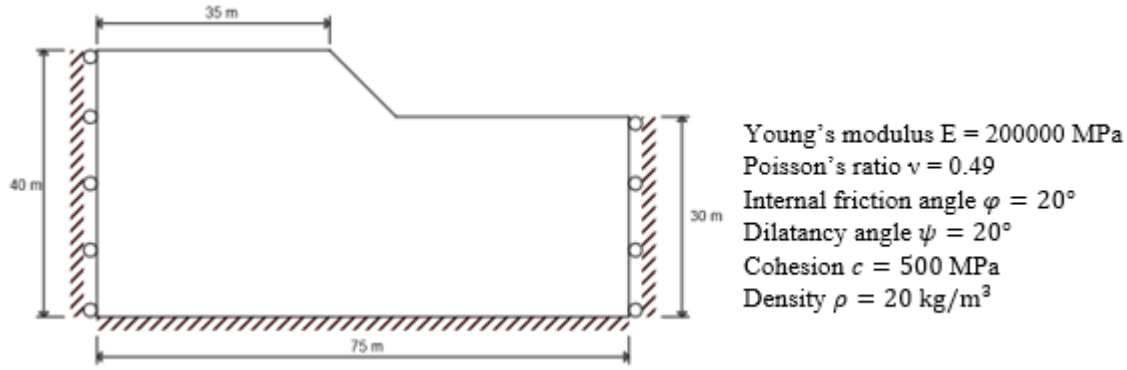

FIGURE 9. Computational model of the slope

The analysis of slopes loaded by self-weight was carried out by Chen [23]. For the given geometric and material parameters, slope failure occurs when the factor

$$N=h\frac{\gamma}{c}=4 \tag{16}$$

reaches its critical value. Here, h is the slope height, and $\gamma=\rho g$ is the unit weight.

The analytical safety factor is defined as follows:

$$\alpha_{\lim}=\frac{N_s}{N}\approx 4.045. \tag{17}$$

For the considered example, $N_s \approx 16.18$.

A gravitational load was applied to the slope: $\bar{g}=\alpha g$. (18)

The parameter α is increased gradually until the solution diverges. The obtained safety factor $\alpha_{\lim}^{\text{fe}} \approx 4.28$ is 5.8% higher than the analytical value.

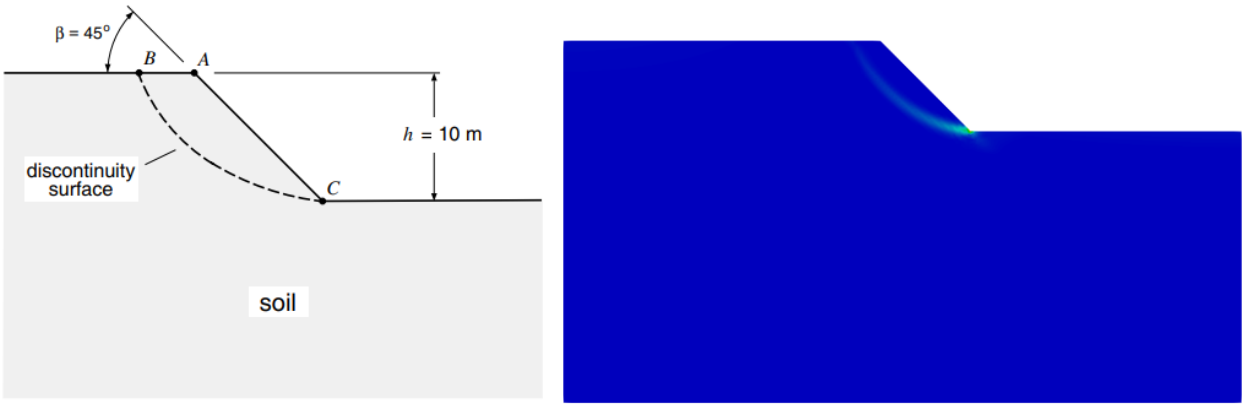

(a) (b)

FIGURE 10. Analytical (a) and numerical (b) solution for the shear band inside the slope

Fig. 10 shows the plastic strain field at the slope instability. The resulting shear band agrees well with the analytical solution (logarithmic curve) [23].

Tension of a Strip with a Circular Hole

In the following example a dependence of the plastic shear band inclination near a circular hole (Fig. 11) on the internal friction angle is analyzed. The Mohr–Coulomb plasticity criterion is used.

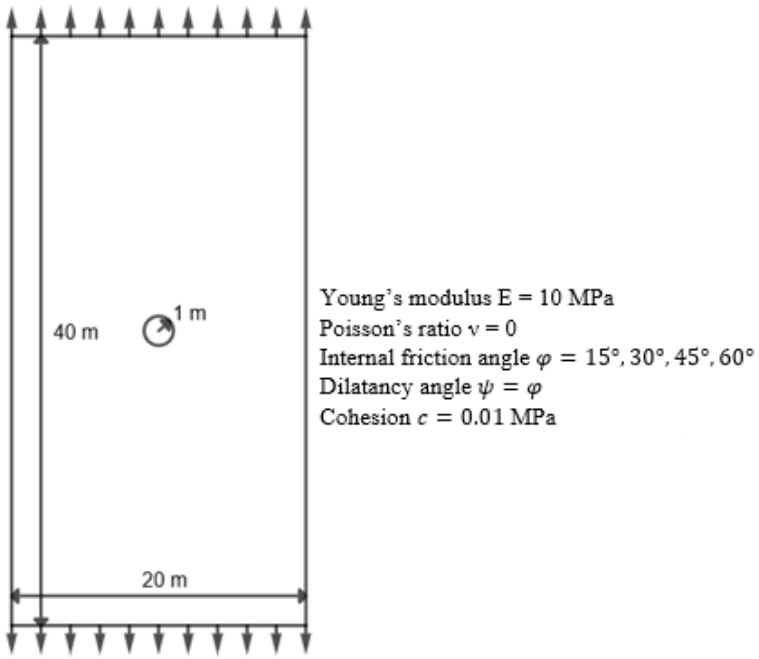

FIGURE 11. Computational model of the strip with a circular hole

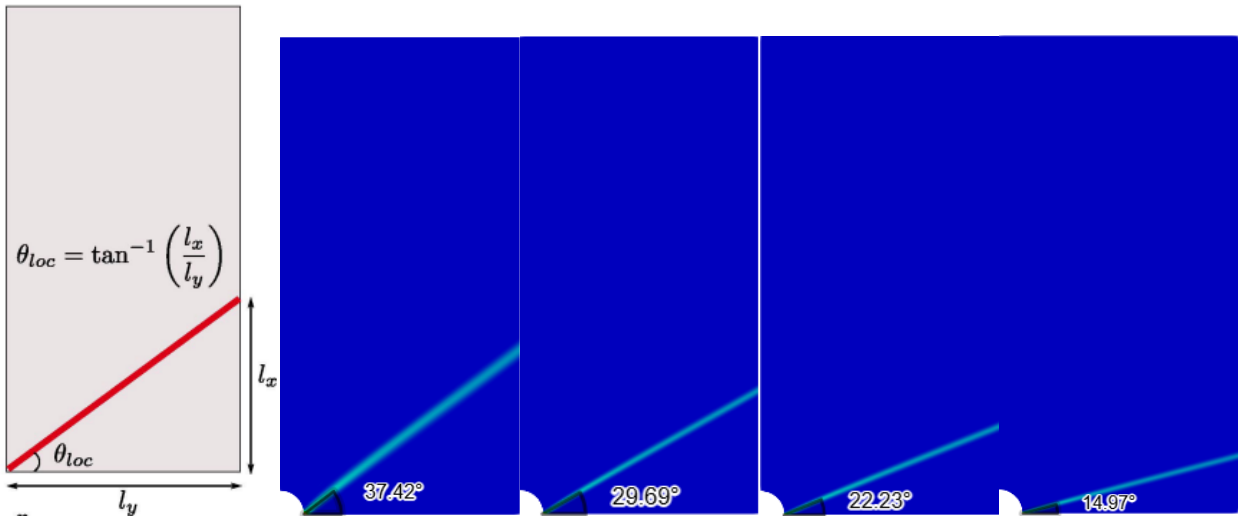

FIGURE 12. Shear band inclination angles for materials with internal friction angles of 15°, 30°, 45°, and 60° (from left to right)

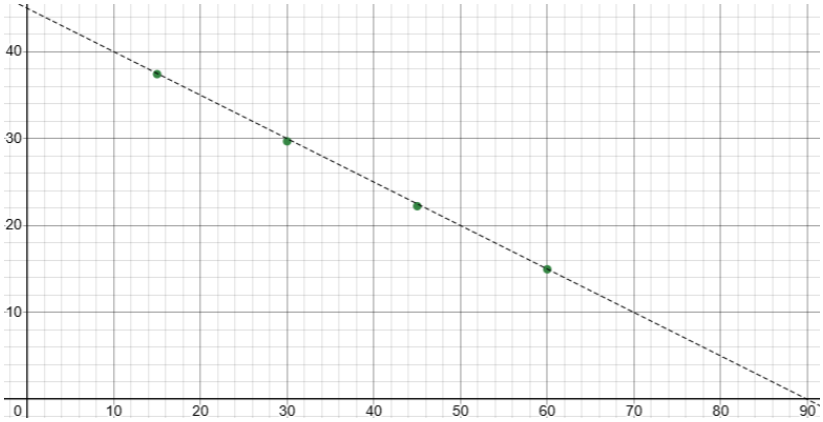

FIGURE 13. Comparison of the internal friction angle vs shear band inclination angle for the analytical (solid line) and numerical (dots) solutions.

Figure 12 demonstrates the shear bands for different angles of internal friction. For the considered case of a strip with a circular hole, plastic shear bands are straight lines inclined to the axis of symmetry at an angle that depends on the material parameters (angle of internal friction). The graph in Fig. 13 demonstrates excellent agreement with the analytical solution [24].

CONCLUSION

High-precision modeling of the rock deformation during the development of a reservoir and geotechnical works plays an important role in modeling various multiscale and multiphysical processes, such as deformation of geological layers, subsidence of the free surface, stability of the wellbore and quarry walls, sand flow, closure/opening of pores, shear deformation along a fault, hydrocarbon production etc. In the modeling of hydrocarbon production, the following main areas can be particularly stressed, in which the consideration of geomechanical processes and their correct description based on modern numerical methods can significantly improve the efficiency of technological operations carried out at the reservoirs: modeling of drilling processes, hydraulic fracturing and geomechanical modeling of the reservoir during its development.

The paper considered models and methods for the geomechanical simulation integrated into the engineering analysis software CAE Fidesys (www.cae-fidesys.com) for solving problems of geotechnical, oil and gas and mining engineering. Examples of solved problems using the Mohr-Coulomb, Hooke-Brown mathematical models used in practice to describe the deformation of rocks and soils were considered. Simulation of plastic shear banding in rocks clearly demonstrated that the spectral element method produces a numerical solution in good agreement with the analytical solution and provides higher-quality results in comparison with the finite element method.

The presented approach makes it possible to address a wide range of geomechanical problems, including the formation and development of plastic shear bands.

ACKNOWLEDGMENTS

The research for this article was performed in Lomonosov Moscow State University and was financially supported by the Ministry of Education and Science of the Russian Federation as part of the program of the Moscow Center for Fundamental and Applied Mathematics under the agreement №075-15-2019-1621.

REFERENCES

1. P. M. A. Areias and T. Belytschko, Two scale shear band evolution with adaptive bandwidth by local partition of unity. International Journal for Numerical Methods in Engineering, in Press.
2. W-F. Chen and E. Mizuno, *Nonlinear Analysis in Soil Mechanics. Theory and Implementation*. (New York: Elsevier 1990).

3. J. R. Rice, A Path Independent Integral and the Approximate Analysis of Strain Concentration by Notches and Cracks. J. Appl. Mech., **35**, 379–386, (1968).
4. I. Vardoulakis, M. Goldscheider and G. Gudehus, Formation of shear bands in sand bodiesas a bifurcation problem. International Journal for numerical and analytical methods in geomechanics, **2**, 99–128, (1978).
5. T. Belytschko, J. Fish and B. Englemann, A finite element method with embedded localization zones. Computer Methods in Applied Mechanics and Engineering, **70**, 59–89, (1988).
6. F. Armero and K. Garikipati. An analysis of strong discontinuities in multiplicative finite strain plasticity and their relation with the numerical simulation of strain localization in solids. International Journal of Solids and Structures, **33**(20-22), 2863–2885, (1996).
7. J. Oliver, M. Cervera and O. Manzoli, Strong discontinuities and continuum plasticity models: the strong discontinuity approach. International Journal of Plasticity, **15**, 319– 351, (1999).
8. M. Ortiz, Y. Leroy and A. Needleman, Finite element method for localized failure analysis. Computer Methods in Applied Mechanics and Engineering, **61**(2), 189–214, (1987).
9. Q. Yang, A. Mota, and M. Ortiz, A class of variational strain-localization finite elements. International Journal for Numerical Methods in Engineering, **62**(8), 1013–1037, (2005).
10. R. A. Regueiro and R. I. Borja, Finite element analysis of strain localization in geologic materials taking a strong discontinuity approach. John A. Blume Earthquakt Engineering Center, **14**, (1998).
11. O. C. Zienkiewicz and R. L. Taylor, *The Finite Element Method.* Volume II: Solid Mechanics. 5th edn. (Butterworth–Heinemann, 2000).
12. F. M. A. Pires, E. A. de Souza Neto and D. R. J. Owen, On the Finite Element Prediction of Damage Growth and Fracture Initiation in Finitely Deforming Ductile Materials. Comp. Meth. Appl. Mech. Engng, **193**, 5223–5256, (2004).
13. F. Zhou and J.F. Molinari, Dynamic crack propagation with cohesive elements: a methodolgy to address mesh dependence. International Journal for Numerical Methods in Engineering, **59**(1), 1–24, (2004).
14. K. A. Petrovskiy, A. V. Vershinin, V. A. Levin, Application of spectral elements method to calculation of stress-strain state of anisotropic laminated shells // IOP Conf. Series: Materials Science and Engineering. Vol. **158**. P. 012077, (2016). http://iopscience.iop.org/article/10.1088/1757-899X/158/1/012077
15. D. Konovalov, A. Vershinin, K. Zingerman, V. Levin, The implementation of spectral element method in a CAE system for the solution of elasticity problems on hybrid curvilinear meshes // Modeling and Simulation in Engineering. (2017), art. id. 1797561. https://doi.org/10.1155/2017/1797561
16. A. A. Markin, D. V. Khristich, Nonlinear Theory of Elasticity: Textbook. 2nd ed. (Tula State University Press, Tula, 2007), 92 p. (in Russian).
17. L. I. Sedov, Continuum Mechanics, Vol. 2. (Moscow: Nauka, 1970), 568 p. (in Russian).
18. A. I. Lurie, Nonlinear Theory of Elasticity, (Moscow: Nauka, 1980). 512 p. (in Russian).
19. L. M. Kachanov, Fundamentals of the Theory of Plasticity, (Moscow: Nauka, 1969). 421 p. (in Russian).
20. E. A. de Souza Neto, Dj. Peric, D. R. J. Owen, Computational Methods for Plasticity: Theory and Applications, (Wiley, 2008), P. 816.
21. A. P. Green, A Theory of the Plastic Yielding Due to Bending of Cantilevers and Fixed-ended Beams, Part I. J. Mech. Phys. Solids, **3**, 1–15, (1954).
22. R. Hill, The Mathematical Theory of Plasticity, (Oxford University Press, London,1950).
23. W-F. Chen, Limit Analysis and Soil Plasticity, (New York, Elsevier, 1975).
24. V. Tvergaard, Influence of Voids on Shear Band Instabilities under Plane Strain Conditions, Int. J. Fract., **17**, 389–407, (1981).
25. A. Vershinin, Poroelastoplastic modeling of a borehole stability under small and finite strains using isoparametric spectral element method. Continuum Mechanics and Thermodynamics, (2022). DOI: http://dx.doi.org/10.1007/s00161-022-01117-4
26. P. A. Vermeer, R. de Borst, Non-associated Plasticity for Soils, Concrete and Rock, Heron. V. **29**, No. 3, P. 1–64, (1984).
27. V. M. Yarushina, & Y. Y. Podladchikov, (De)compaction of porous viscoelastoplastic media: Model formulation, J. Geophys. Res. Solid Earth **120**, 4146–4170 (2015).
28. Y. P. Stefanov, M. A. Chertov, G. R. Aidagulov, A. V. Myasnikov, Dynamics of inelastic deformation of porous rocks and formation of localized compaction zones studied by numerical modeling, J. Mech. Phys. Solids. V. **59**, No. 11, P. 2323–2340, (2011).
29. C. Carranza-Torres, “Elasto-plastic solution of tunnel problems using the generalized form of the Hoek-Brown failure criterion”, Int. J. Rock Mech. Min. Sci., **41**, no. SUPPL. 1, 629-639, (2004).